Disclaimer

The report at hand was written in the course of the respective class at the University of Bonn. If not stated differently on top of the first page or the following website, the report was prepared and handed in solely by me, Marvin Zanke. Any handwritten annotations are usually corrections that I or a tutor made. For more information and all my material, check: https://www.physics-and-stuff.com/

I raise no claim to correctness and completeness of the given report! This equally applies to the corrections mentioned above.

Advanced Laboratory Course

A248: Magneto-Optical Trap

Group P8

Marvin Zanke
s6mazank@uni-bonn.de

Fabian Müller
s6fnmuel@uni-bonn.de

October 04/05, 2018

Contents

Abstract

In this experiment, we set up a magneto-optical trap, which combines radiation pressure and a quadrupole magnetic field in order to cool down atoms and further catch them at a confined spot in space. The experimental setup uses several mirrors, waveplates and polarizing beam splitters.

The experiment is carried out on two days. On the first day, we try to tune the frequencies of the used lasers and adjust the beams such that we can detect the magneto-optical trap, i.e. caught atoms, upon turning on the magnetic field.

On the second day, we determine several characteristics of the magneto-optical trap. These characteristics are the population and size of the magneto-optical trap, the influence of the used quarter waveplates' angle and the current in the magnetic coils on the fluorescence power of the magneto-optical trap, as well as the loading behavior of the magneto-optical trap.

1 Theory

If not mentioned explicitly, the theory is based on the references [1] and [2].

1.1 Experimental setup of a Magneto-Optical Trap

In order to construct a *magneto-optical trap (MOT)*, one needs a *laser system* and a *MOT part*, shown in figure 1.1. The laser light from the experimental laser system setup is coupled into an optical fibre and guided to the MOT setup.

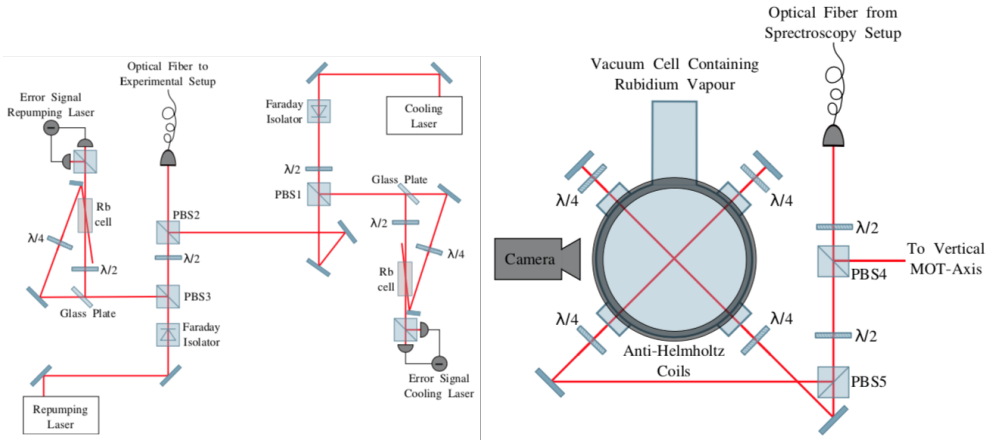

Figure 1.1.: The left figure shows the sketched experimental setup of the laser system and the right figure the sketched experimental setup of the MOT. *PBS* stands for a *polarizing beam splitter*. Figures taken from [1].

In order to stabilize the frequencies of the *cooling and repumping laser*, the experimental setup uses two *Rubidium cells* for *spectroscopy*, where the beams used for the spectroscopy have a small intensity and originate from splitting the initial beams. Most part of the intensities from the lasers are coupled into an optical fiber and guided to the MOT setup.

In the MOT, the light is split into three parts and directed onto the *vacuum cell*, each part covering one spatial direction. The vacuum cell is filled with Rb^{85} and Rb^{87} atoms and surrounded by a set of *coils* in *anti-Helmholtz configuration*, giving rise to a *quadrupole magnetic field*.

1.2 Laser

For this experiment, a tunable laser that can be stabilized at a specific frequency is needed. Therefore, a *laser diode* in *Littrow configuration* is used, as depicted in figure 1.2. Here, the light of a laser diode with a bright spectrum is collimated onto a grating with the help of a lens. The grating can be adjusted using a piezo and is aligned such that the $(-1)^{\text{st}}$ order of the desired frequency is reflected back into the resonator of the laser – inducing stimulated emission – while the zeroth order has most of the power and leaves the laser.

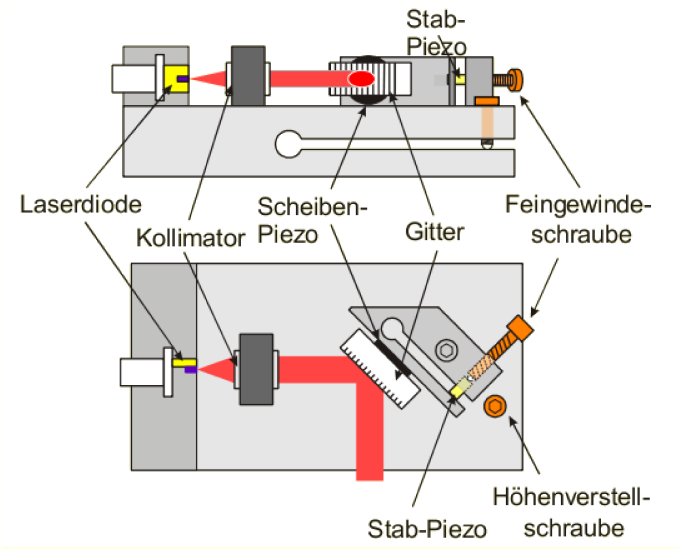

Figure 1.2.: Littrow configuration of the laser diode. Figure taken from [1].

Due to temperature differences and vibrations, the laser frequency can drift, such that an *error signal* is applied to the piezo for a stabilization of the frequency. The error signal can be obtained by *Doppler-free spectroscopy*, as explained in the next section, section 1.3.

1.3 Doppler free spectroscopy

Due to movement of the atoms in regular spectroscopy, only a *Doppler-broadened spectrum* can be observed. Therefore, *saturation spectroscopy* is used. Here, the laser beam is split into a powerful *pump beam* and a *test beam* of lower intensity, passing the sample in opposite directions. The test beam is then measured with a photodiode, resulting a *transmission spectrum*.

For simplicity, a two level system is discussed in the following which can easily be generalized. Blocking the pumpt beam, a regular Doppler-broadened spectrum can be observed, showing a peak at the atomic resonance frequency as seen in the left figure 1.3. Turning on the pump beam, a narrow spike appears at the resonance, the so-called *Lamb dip*, as seen in the right figure 1.3. This peak is coming from atoms moving with velocity $v = 0$ with respect to the beam axis, making the frequencies of pump and test beam appear equal to the atoms. Due to the high intensity of the pump beam, the ground state is occupied significantly less, leading to a lower absorption of the test beam. Therefore, the Lamb dip exhibits the natural line width. This does not happen for other velocity classes, where one beam gets blue- and the other one redshifted. Due to these shifts, *crossover peaks* can be observed in multi-level systems.

Polarization spectroscopy uses this principle in an advanced setup. Here, the pump beam is *circularly polarized*, resulting in an unequal population of the degenerate m_F states. The linear polarized test beam can be thought of as a superposition of both circular polarizations. Due to the higher occupation of one of these states, the sample acts *birefringent*. In the setup used in this experiment, the outgoing test beam is split in a PBS and the two spectra get subtracted. The resulting signal is proportional to the change in the refractive index, which has a similar behavior as the derivative of the absorption profile (*Kramer-Kronig relation*). This signal is perfectly suited as an error signal for the lasers.

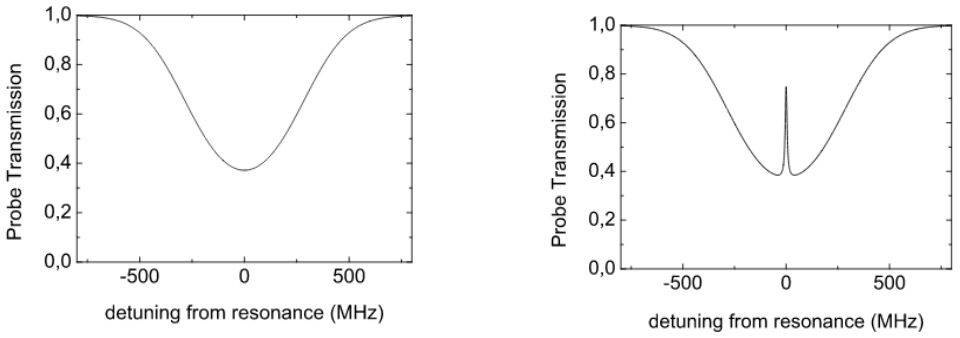

Figure 1.3.: A transmission spectrum from Doppler-free saturation spectroscopy in a two level model. Left: Only one beam. Right: Pump and test beam. Figures taken from [3].

1.4 Optical Cooling and the Magneto-Optical Trap

When a photon is resonant with a transition between two energy levels of an atom, it can get absorbed by the atom and transfer its momentum $p = \hbar k$ to the atom. Upon relaxation of the atom and the subsequent emission of a photon, this effect will also give a recoil momentum to the atom.

A resonant laser beam guided onto an atom thus gives rise to the so-called *radiation pressure* $F = dp/dt$, while the *isotropic photon emission* results in a random walk, with the forces summing up to approximately zero. As we want to slow down atoms and not accelerate them, we have to consider the Doppler-effect and detune our laser slightly to the red, such that 'only' oncoming atoms feel this radiation pressure. This scenario is sketched in figure 1.4.

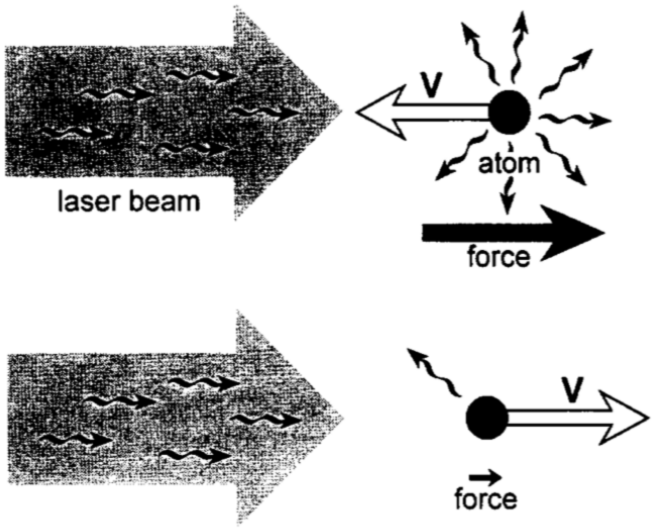

Figure 1.4.: The two cases of a red-shifted laser impinging on an atom moving towards the laser and an atom moving away from the laser. The force on the former one is larger due to its resonance concerning the cooling transition because of the Doppler-effect. Figure taken from [2] and slightly edited.

By applying laser beams from all six directions (three pairs counterpropagating each), one can use this effect to cool a bunch of atoms, i.e. reduce their average velocity and hence temperature, forming a cloud of atoms. This setup is the so-called *optical molasses*. Yet, the mentioned recoil from the emitted photons imposes the so-called *Doppler-limit* onto this cooling, arising from a balance between heating and cooling rate.

The cooled atoms can and will still diffuse out of the optical molasses due to their remaining velocity. Resorting to the *Zeeman effect* by applying a quadrupole magnetic field B – generated by two coils in anti-Helmholtz configuration – we can add a position-dependence to the force. The magnetic field should have its zero point in the middle of the beam's intersection volume, with a linearly in-/decreasing magnetic field in every beams's direction. This setup is then referred to as a magneto-optical trap (MOT). While in the middle of the MOT ($B = 0$), the cooling force remains the same, the degeneracy of the energy levels of an atom drifting away from this point is removed and its resonance gets shifted towards the frequency of the red-detuned laser beam, as depicted in figure 1.5 for one dimension – note here, that in our case the M_J states correspond to m_F hyperfine states . It is then clear, that we have to use circular polarized light, such that the proper beam can be absorbed and slow down the atom, instead of accelerating it. This will be σ^+-polarized light from the side with a negative magnetic field in order to excite the resonant $m_F = 1$ state and vice versa for σ^--polarized light from the positive magnetic field's side. The respective differently polarized light will not be resonant and thus not accelerate the atom – note, that $\sigma^\pm$-polarized light can only excite the $m_F = \pm 1$ state.

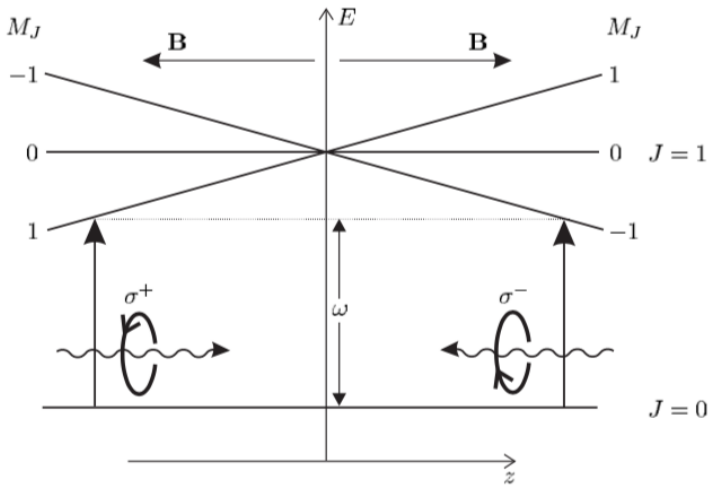

Figure 1.5.: A one-dimensional explanation of the principle of a MOT. The degeneracy is removed by the magnetic field, splitting the energy levels into $m_F = 1, 0, -1$. Red-shifted, opposite circular polarized light is then used, in order to be resonant with the correct Zeeman-shifted transition and effectively confine the atoms in space. Figure taken from [5]. Note that in our case it should be m_F instead of M_J.

1.5 Rubidium MOT

There exist two stable isotopes of Rubidium, Rb^{85} and Rb^{87}. In this experiment, we catch Rb^{85} atoms in the MOT, with the Rb^{87} being around in both, the vacuum chamber and the spectroscopy cell. The level system of Rb^{85} is depicted in figure 1.6, where we choose the $F = 3 \rightarrow F' = 4$ transition for the cooling. It is *nominally closed*, which means that the atoms in the excited state can only decay back into the ground state of this transition. Still, an off-resonant excitation $F = 3 \rightarrow F' = 2, 3$ may happen in some cases, allowing the atom to decay to the $F = 2$ ground state. In this state, the used laser light is highly detuned from any available excitation, making it impossible to further cool it down. What one does here, is use a second laser, emitting light resonant with the $F = 2 \rightarrow F' = 3$ transition and thus *repumping* the atoms to the cooling transition upon decay into its ground state.

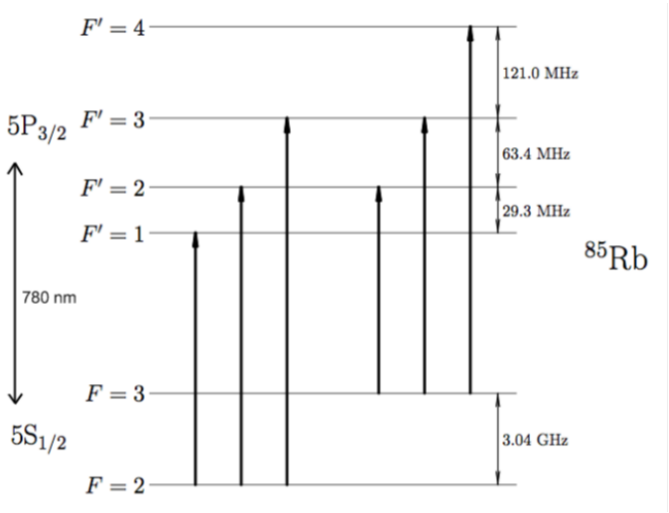

Figure 1.6.: A part of the Rb^{85} level scheme with the different hyperfine transitions occurring in this experiment. Figure taken from [1].

1.6 Error Function and Gaussian Profile

In this experiment, we will fit the integral of a gaussian function given by

$$I(r) = I_0 \exp\left(\frac{-2r^2}{w^2}\right)$$

to our measured data. The integral will then be given by

$$P(\hat{x}) = I_0 \int_{-\infty}^{\infty}\int_{\hat{x}}^{\infty} \mathrm{d}\bar{x}\,\mathrm{d}y\, \exp\left(\frac{-2y^2}{w^2}\right) \exp\left(\frac{-2\bar{x}^2}{w^2}\right) = P_0 - P_0 \,\mathrm{erf}\left(\frac{\sqrt{2}}{w}\hat{x}\right), \quad (1.1)$$

where $P_0 = -\frac{1}{4} I_0 \pi w^2$ and $\hat{x} = x - x_0$, with x_0 the center of the intensity distribution. Plotting the error function $\mathrm{erf}(x)$, one finds figure 1.7.

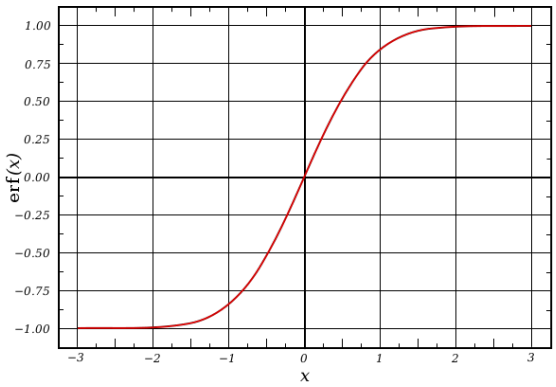

Figure 1.7.: A plot of the error function $\mathrm{erf}(x)$. Figure taken from `https://en.wikipedia.org/wiki/Error_function`.

The used intensity distribution above, is the intensity distribution of a gaussian beam. It possesses a so-called gaussian profile, depicted in figure 1.8.

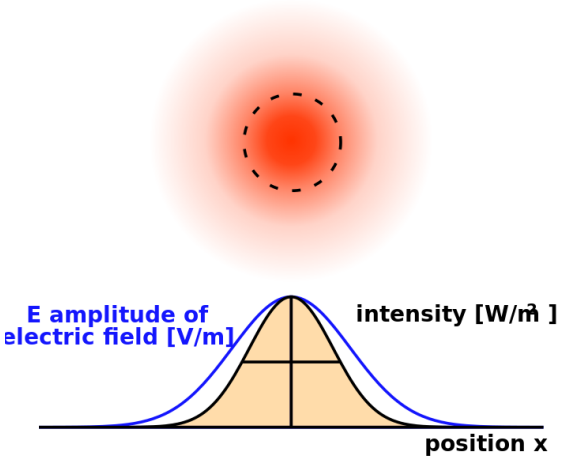

Figure 1.8.: The profile of a gaussian beam, with maximum intensity in the center, but a non-vanishing intensity at infinity. Figure taken from `https://en.wikipedia.org/wiki/Gaussian_beam`.

This theory part is of course only a short summary and presumes that the reader has some basic knowledge of those concepts. For more details, we can recommend the paper [2], on which this recap is partly based on. To understand all the details and underlying theoretical background, we find the books [4] and [5] useful.

2 Experimental Analysis

2.1 Experimental Setup and Calibration

In order to characterize the magneto-optical trap (MOT) in the later course of the experiment, we first have to calibrate the experimental setup. To that end, we are given the properly aligned experimental setup of the laser system mentioned in the theory part and shown in figure 2.1.

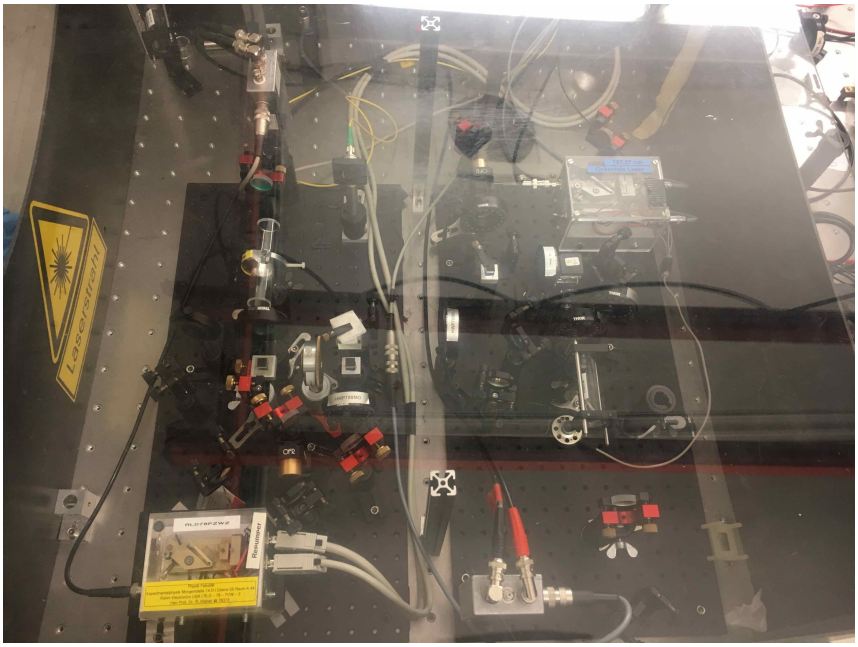

Figure 2.1.: The experimental setup of the laser system with a cooling laser, a repumping laser and the two spectroscopy cells, including several mirrors, polarizing beam splitters, waveplates and an optical fiber to the experimental MOT setup.

Further parts of the experimental setup that are not to be touched is the breakable vacuum cell of the MOT setup including the pumps, and the items fixed onto the optical table like e.g. the postholders, the quarter waveplates, the beamsplitters, the camera and the magnetic coils. The MOT setup with the corresponding beam paths is shown in figure 2.2.

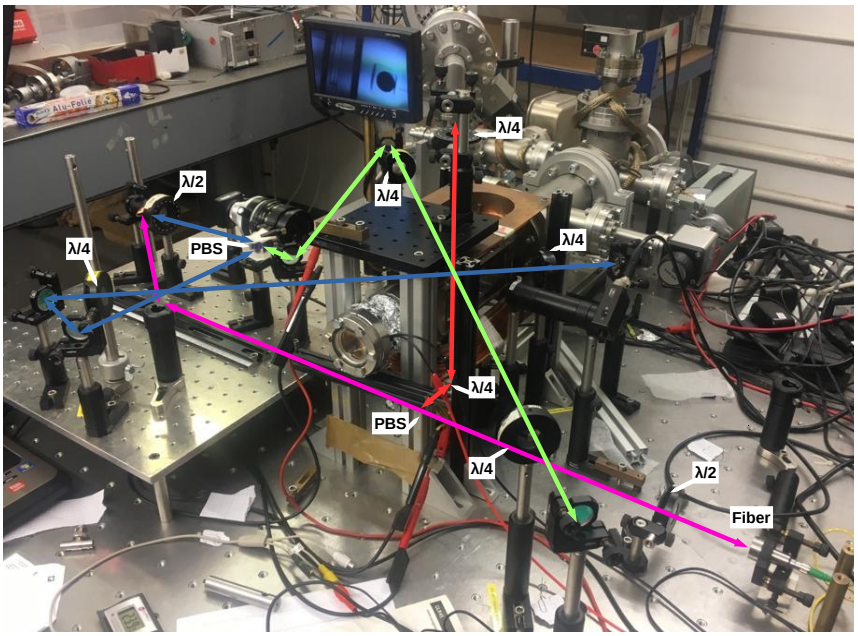

Figure 2.2.: The experimental MOT setup with the light coming out of the optical fiber from the laser system setup. The MOT setup includes several mirrors, polarizing beam splitters, waveplates and a fixed digital camera. Sketched are the paths of the different laser beams and their way through the vacuum chamber.

The laser beams carried to the experimental MOT setup through the optical fiber then have to be tuned to the correct frequencies and adjusted properly with the help of the mirrors and the $\lambda/2$ waveplates in the MOT setup. At first, the tutor sets the temperature of the laser diodes to an appropriate value and also gives an estimated value for the required laser diode's currents. With both, the repumping and cooling laser on scan mode, we then tune the amplitude of the feedback signal to a maximum, an offset scan voltage and the diode current until we find the Rb^{85}-spectrum on the oscilloscope. At this point, we are able to see fluorescence from the yet to be aligned laser beams in the vacuum chamber. We then check the light power that is passing through the optical fiber and split the power in the experimental MOT setup such that each of the three laser beams in the three axes has an equal amount of power. To that end, we turn off the repumping laser and use a power meter to measure the power of the cooling laser directly after the optical fiber, after the first polarizing beam splitter (PBS) and after the second PBS (see figure 2.2). Turning the $\lambda/2$ waveplates in front of the PBSs, we can then change the amount of power that is split by the PBSs and equal them to approximately 2.2 mW each. The power meter device is shown in figure 2.3.

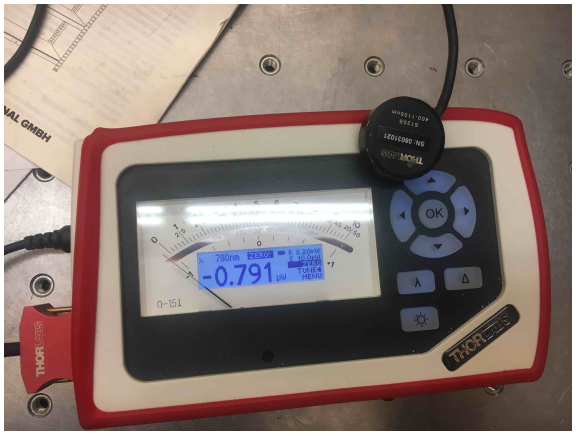

Figure 2.3.: The optical power meter used in this experiment, consisting of the sensor and a display.

The hardest part of setting up the MOT is yet to come. As written in [1], 'setting up the MOT can be like looking for a needle in a haystack', which includes the adjustment of the MOT beams. The seven mirrors visible in figure 2.2 have to be adjusted such that the three laser beams and the back-reflections of these cross in the middle of the vacuum chamber. We start off with the adjustment of the mirrors from the point of the incoming beam at the optical fiber and then go over the the mirrors responsible for the back-reflections. It is really important, that all the beams cross in the middle – where the magnetic field vanishes – and that the back-reflections overlay the incoming beams all the way back to the fiber. Besides a small, mobile camera (sensitive to infrared 780 nm light) with a display shown in figure 2.4, we have a fixed digital camera (also sensitive to infrared light) connected to a laptop display as seen in figure 2.5 at hand. In order to check the exact overlay of the incoming and back-reflected beams, we use a small sheet with a hole in it, such that the hole is held in front of the incoming beam and possible back-reflected beams may be seen on the sheet right next to the hole if they do not exactly overlay. If the laser beams are adjusted and the frequencies of the lasers tuned properly, one should be able to see caught atoms in the MOT upon locking the lasers to the desired frequencies, switching on the MOT coil's power supply (for now, the current value is supposed to be at its maximum of $I_{\text{coils}} = 5.2\,\text{A}$) and detuning the cooling laser's frequency slightly to a lower frequency (red-shift) with the input offset. Note here, that the detuning is necessary because of the Doppler-effect mentioned in the theory part. Turning the repumping laser's frequency with the input offset knob, we can optimize the fluorescence. During the calibration of the experiment, we use a permanent magnet to apply a magnetic offset field, in order to check whether the problem of a non-working MOT is the exact overlay of the laser beams in the

middle of the vacuum chamber, or the zero point of the magnetic field not being in the middle of the laser beam's crossing.

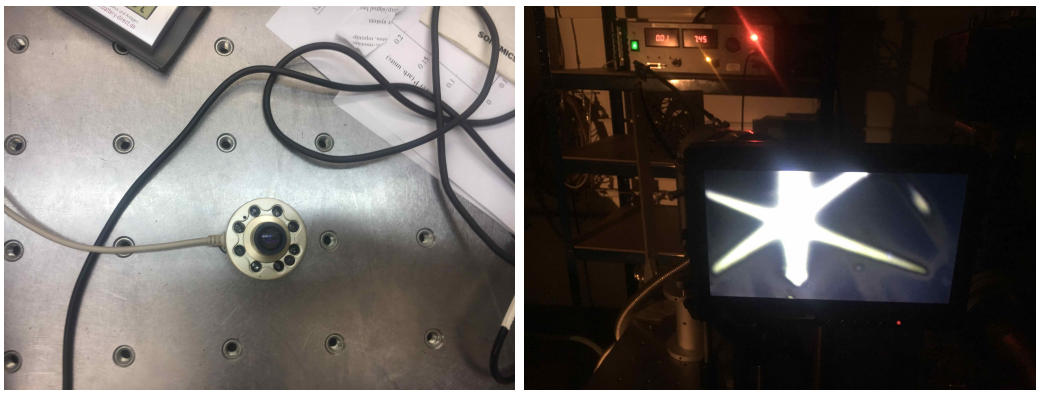

Figure 2.4.: The small, mobile camera used in this experiment in order to properly align the laser beams in the middle of the vacuum chamber and the corresponding screen display.

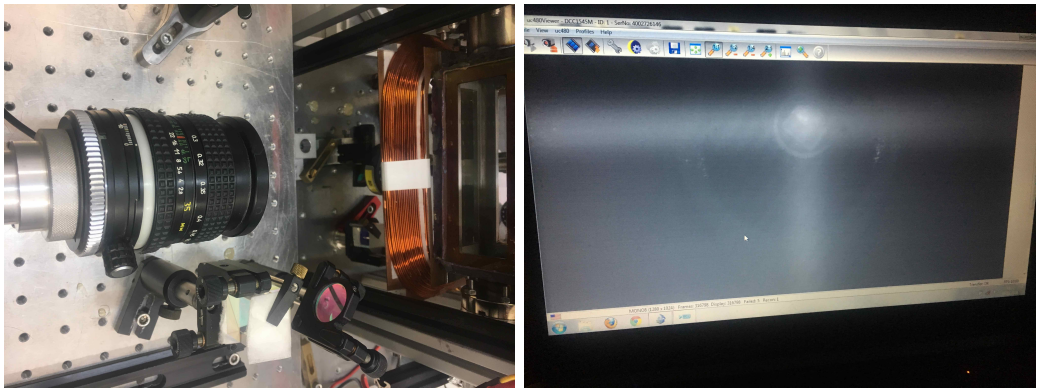

Figure 2.5.: The digital camera which we use in this experiment, fixed on the optical table, and the display of the laptop showing the view of the camera.

Having set up the MOT properly, we continue to the main part of the experiment, which is determining several MOT characteristics. For this, we use the power meter to detect the MOT fluorescence, where we image the MOT onto the power meter with the help of a lens. Note, that one has to subtract a background from the measurements with the power meter, i.e. subtract the value on the power meter with turned off magnetic field from the MOT measurements with turned on magnetic field. If not stated differently, the errors are obtained by gaussian error propagation.

2.2 MOT Population

In the first part of this experiment, we want to determine the number of atoms caught in the MOT – the so-called MOT population. The required parameters are the fluorescence value of the MOT, the lens diameter, the distance between the lens and the MOT, the detuning of the cooling laser (will be determined in a later part of the experiment), as well as the beam power and diameter. We fix the power meter at the end of a tube with length $2f$ (f being the focal length of the lens), such that the light is focussed in its focal point. In order to subtract the background, we turn off the magnetic field and press the off-set button on the power meter before measuring with the turned on magnetic field.

2.2.1 Fluorescence Power

Using the power meter fixed at the end of the tube, we measure the power of the MOT three different times because of the fluctuating values. We find

$$P_{\mathrm{pm},1} = (150 \pm 10)\,\mathrm{nW}, \qquad P_{\mathrm{pm},2} = (150 \pm 5)\,\mathrm{nW}, \qquad P_{\mathrm{pm},3} = (144 \pm 10)\,\mathrm{nW}.$$

Calculating the mean of these values with the variance weighted method explained in the appendix A, we find

$$P_{\mathrm{pm}} = (149 \pm 4)\,\mathrm{nW}. \tag{2.1}$$

The total power of the MOT can then be calculated by considering the MOT in the center of a sphere and the lens on the surface of this sphere as depicted in figure 2.6.

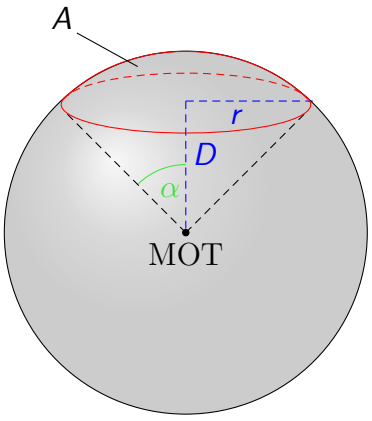

Figure 2.6.: A sphere with the MOT in the center and the lens coating the part A of the sphere with the solid angle Ω. The figure was created in TikZ, following [6], where we slightly changed the code for our purpose.

Having the formulas

$$\cos\alpha = \frac{D}{\sqrt{D^2+r^2}},$$
$$A = \int_0^{\alpha}\int_0^{2\pi} \mathrm{d}\phi\,\mathrm{d}\theta\,(D^2+r^2)\sin\theta = 2\pi(D^2+r^2)\left(1-\frac{D}{\sqrt{D^2+r^2}}\right),$$
$$\Omega = \frac{A}{D^2+r^2} = 2\pi\left(1-\frac{D}{\sqrt{D^2+r^2}}\right),$$

and using the measured value $D = (9.0 \pm 0.5)\,\mathrm{cm}$ for the distance from the MOT to the lens, as well as the given value $2r = 2.54\,\mathrm{cm}$ for the diameter of the lens, we find

$$\Omega = (0.0616 \pm 0.0067)\,\mathrm{sr}. \tag{2.2}$$

Given the value for P_{pm} in eq. (2.1) and eq. (2.2), we obtain the total power of the MOT to be

$$P_{\mathrm{tot}} = \frac{4\pi}{\Omega} P_{\mathrm{pm}} = (30.4 \pm 3.4)\,\mu\mathrm{W}. \tag{2.3}$$

2.2.2 Detuning of the Laser Frequencies

In section 2.7, we will determine the detuning of the cooling laser to be

$$\Delta = (13.1 \pm 2.1)\,\mathrm{MHz}. \tag{2.4}$$

2.2.3 Beam Power and Diameter

Before determining the beam diameter, we measure the beam power of the cooling laser by turning off the repumping laser and use the power meter at the fiber output once more. This results in

$$P_{\mathrm{beam}} = (6.7 \pm 0.1)\,\mathrm{mW}. \tag{2.5}$$

In order to measure the beam diameter, we make use of a razor blade on an optical rail. One then records the beam power in dependence of the blade's position and fits the integral over the gaussian beam – the so-called error function – to these values. Assuming a gaussian profile for the laser beam, we use the formula

$$I(r) = I_0 \exp\left(\frac{-2r^2}{w^2}\right)$$

(see [4, p.41]), where $r = \sqrt{x^2+y^2}$, for the intensity and propagation in z-direction. For $r = w$, one gets the $1/e^2$ beam radius, which is the obtainable quantity of

interest. As we measure powers, we yet have to integrate the intensity to obtain the power at the position $\hat{x} = x - x_0$, x_0 being the center of the intensity distribution, yielding

$$P(\hat{x}) = I_0 \int_{-\infty}^{\infty} \int_{\hat{x}}^{\infty} \mathrm{d}\bar{x}\,\mathrm{d}y\, \exp\left(\frac{-2y^2}{w^2}\right) \exp\left(\frac{-2\bar{x}^2}{w^2}\right) = P_0 - P_0 \operatorname{erf}\left(\frac{\sqrt{2}}{w}\hat{x}\right), \quad (2.6)$$

where $P_0 = -\frac{1}{4} I_0 \pi w^2$.

The raw data for the measurement is given in table B.1 in the appendix B and the plot is shown in figure 2.7, with the fit parameter for the beam radius being

$$w = (0.247 \pm 0.061)\,\mathrm{cm}. \quad (2.7)$$

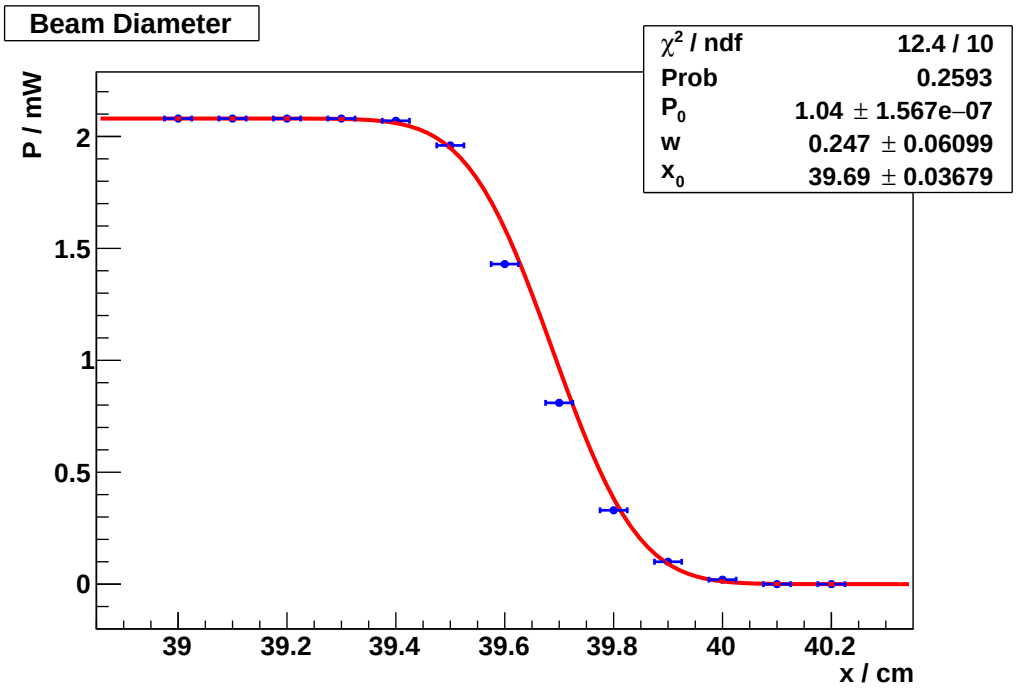

Figure 2.7.: The measured values for the power in dependence of the razor blade's position on the optical rail and a fitted function of the form eq. (2.6) to these values.

2.2.4 MOT Population

Having obtained all the necessary parameters, we are able to determine the number of atoms caught in the MOT. Therefore, we take the formula

$$P_{\text{tot}} = N \cdot R \cdot h \cdot \nu_{\text{c}},$$

giving a relation between the total fluorescence power and the number of atoms N in the MOT, the scattering rate per atom R, as well as the energy of the emitted light $h \cdot \nu_{\text{c}}$ ($\nu_{\text{c}} = 3.843 \times 10^{14}\,\text{Hz}$ being the frequency of the 780 nm cooling transition, see [2]) and solve it for N, yielding

$$N = \frac{P_{\text{tot}}}{R \cdot h \cdot \nu_{\text{c}}}. \tag{2.8}$$

In accordance with [2], the scattering rate per atom can be calculated by

$$R = \frac{(I/I_S)\pi\Gamma}{1 + (I/I_S) + 4(\Delta/\Gamma)^2}, \tag{2.9}$$

where I is the total intensity of the cooling beam (incoming and back-reflected beams), $\Gamma = 6\,\text{MHz}$ the natural linewidth of the cooling transition, Δ the detuning of the cooling laser's frequency from resonance and $I_S = 4.1\,\text{mW/cm}^2$ the saturation intensity. Concerning the total intensity of the cooling beam, we use the total beam power from eq. (2.5) and the beam radius from eq. (2.7) to calculate the intensity (see [7])

$$I = \frac{4P_{\text{beam}}}{w^2\pi} = (139.827 \pm 69.096)\,\text{mW/cm}^2, \tag{2.10}$$

where an additional factor of 2 arises from the back-reflected beam.

Having obtained the value for the total fluorescence power eq. (2.3), the intensity eq. (2.10), the detuning eq. (2.4) and the values for Γ, I_S and ν_{c} given above, we calculate the scattering rate per atom R and the number of atoms caught in the MOT N with the use of eq. (2.9) and eq. (2.8) to be

$$R = (11.87 \pm 2.55)\,\text{MHz}, \tag{2.11}$$

$$N = (1.01 \pm 0.11) \times 10^7\,\text{particles}. \tag{2.12}$$

Comparing this with $N^{\text{lit}} = 4 \times 10^7\,\text{particles}$ (see [2]), we find that it is a typical value for the number of atoms that can be caught in a MOT.

2.3 Size of the MOT

To measure the size of the MOT, we use the laptop to take a screenshot of the fixed camera's view of the MOT, as seen in figure 2.8. Here, we take two screenshots at different times, as the MOT changed after some minutes. The camera is adjusted such that the MOT is as focussed as possible. With the same adjustment, we then take a photo of a ruler, resulting in figure 2.9. Using this figure and an image editing program, we find the correspondence

$$1\,\mathrm{mm} \mathrel{\hat{=}} (30 \pm 1)\,\mathrm{px} \tag{2.13}$$

between length and pixels.

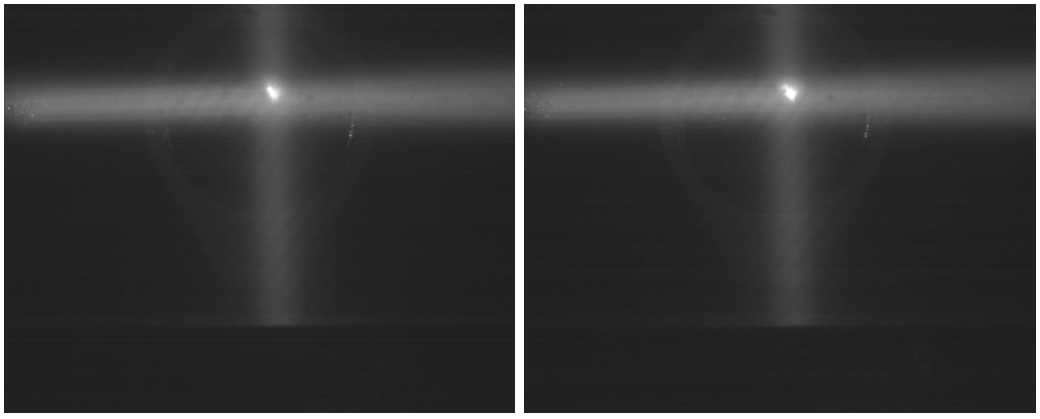

Figure 2.8.: Two screenshots of the MOT, taken with the digital camera. Between the two screenshots, there was a time interval in the magnitude of some minutes, as the MOT changed in shape and size over time.

Figure 2.9.: A screenshot of a ruler, taken with the digital camera. The focus of the digital camera is the same as for the screenshots of the MOT. With this image, we can find the correspondence between length and pixels.

Zooming into figure 2.8 to determine the size of the MOT, we find figure 2.10 and the sizes

$$\begin{aligned} \mathrm{MOT}_1: &\quad (35 \pm 1)\,\mathrm{px} \times (20 \pm 1)\,\mathrm{px}, \\ \mathrm{MOT}_2: &\quad (36 \pm 1)\,\mathrm{px} \times (28 \pm 1)\,\mathrm{px} \end{aligned}$$

in pixels for the two MOTs. Converting the pixels into mm with the help of eq. (2.13), we find the sizes

$$\begin{aligned} \mathrm{MOT}_1: &\quad (1.17 \pm 0.03)\,\mathrm{mm} \times (0.67 \pm 0.03)\,\mathrm{mm}, \\ \mathrm{MOT}_2: &\quad (1.20 \pm 0.03)\,\mathrm{mm} \times (0.93 \pm 0.03)\,\mathrm{mm}. \end{aligned}$$

The second MOT has a round shape, such that we can hypothesize it as a sphere with diameter

$$d = (1.07 \pm 0.03)\,\mathrm{mm}.$$

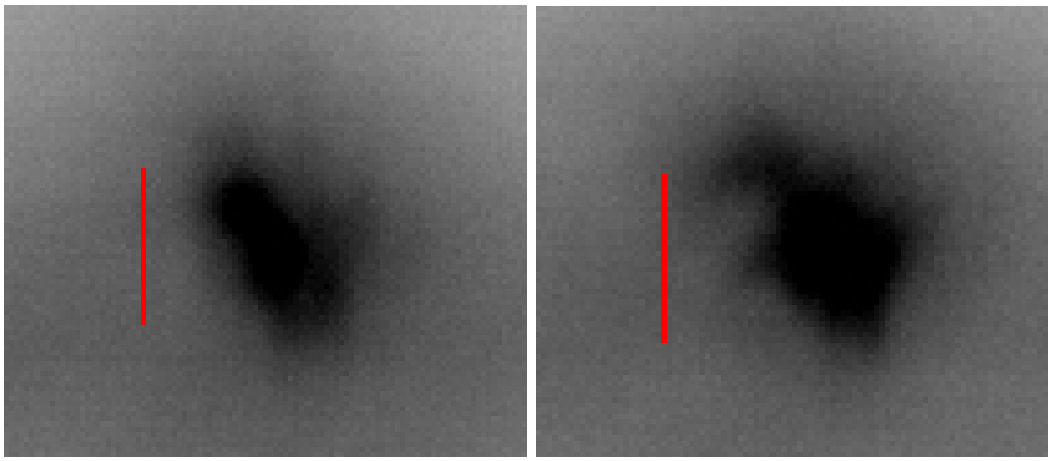

Figure 2.10.: A zoomed-in view of the two screenshots taken from the MOT. The right figure shows a rather round shape. The red lines sketched in the figures represent the length of 1 mm.

2.4 Influence of the quarter waveplates

We now want to investigate the influence of the quarter waveplates on the fluorescence power of the MOT. To that end, we pick one of the three split beams and measure the fluorescence power with the power meter in dependence of the angle of the quarter waveplates in the beam path. We decide for the blue sketched beam, depicted in figure 2.2, and start by changing the angle of the quarter waveplate

that is passed by the incoming and back-reflected beam. We then reset the angle of this quarter waveplate to its initial value 180° and repeat the procedure for the quarter waveplate passed by the back-reflected beam only. After the measurement, this quarter waveplate is also reset to its initial value 180°. The obtained raw data is given in table B.2 and B.3 in the appendix B. Plotting the values in table B.2 for the first quarter wave and fitting a function of the form

$$P(\phi) = C + A\cos^2\big(\phi + \phi_0\big)$$

to the values, we find figure 2.11. We also try to fit a function of the form

$$P(\phi) = C + A\cos^n\big(\phi + \phi_0\big)$$

to these values, resulting in figure 2.12. Remarkable is here, that the fluorescence power does not vanish entirely, which we ascribe to the remaining cooling forces and the trapping in the other two spatial dimensions. The reason for the $\cos^2$-behavior can be justified as follows. We look at the electric field $\vec{E}$ of some arbitrarily polarized light and circularly polarized light

$$\vec{E} = E_0 \begin{pmatrix} \cos\phi \\ -\sin\phi \end{pmatrix} \exp\big(\mathrm{i}(\omega t - kz)\big), \quad \vec{E}_{\mathrm{circ}} = E_0 \begin{pmatrix} \cos\frac{\pi}{4} \\ -\sin\frac{\pi}{4} \end{pmatrix} \exp\big(\mathrm{i}(\omega t - kz)\big).$$

Computing the scalar product of these two vectors, one finds the part of the arbitrarily polarized light, which is circularly polarized, in our case

$$\big(\vec{E}\cdot\vec{E}_{\mathrm{circ}}\big)^2 = \frac{1}{2}\big(1 + \sin 2\phi\big).$$

This is equivalent to a shifted $\cos^2\phi$ and thus justifies the ansatz used above.

Plotting the values in table B.3 for the second quarter waveplate yields figure 2.13, with the power being constant and independent of the second quarter waveplate's angle. The constant behavior is expected here, as the circular polarized light gets linearly polarized by the posterior waveplate, reflected at the mirror and again transformed into circularly polarized light with opposite sense of rotation, thus resulting in no change of the fluorescence.

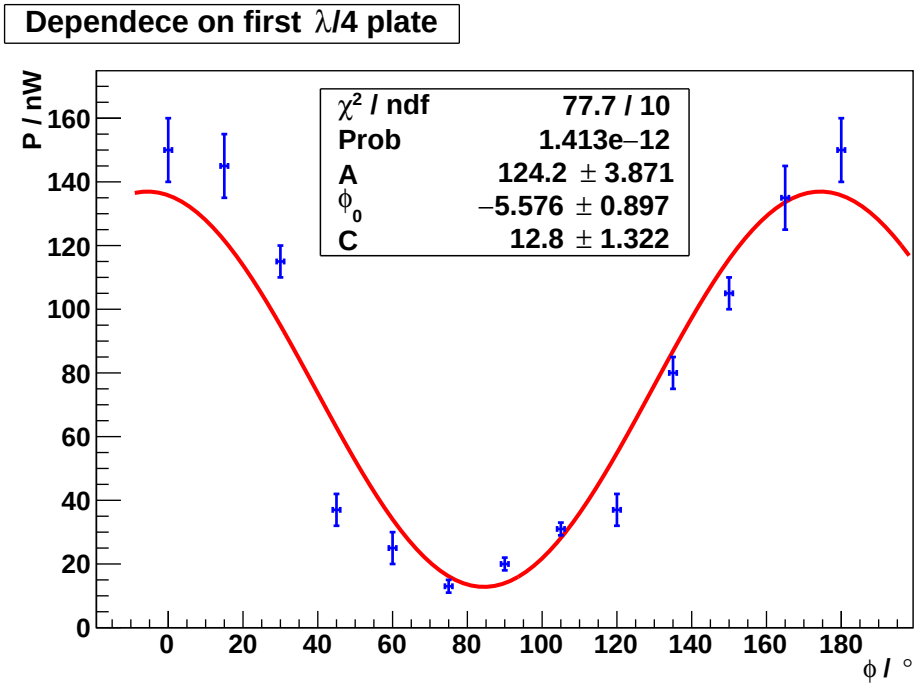

Figure 2.11.: The data obtained for the power in dependence of the angle of the first quarter waveplate and a fitted function to these values with a Malus's law like $\cos^2$-behavior.

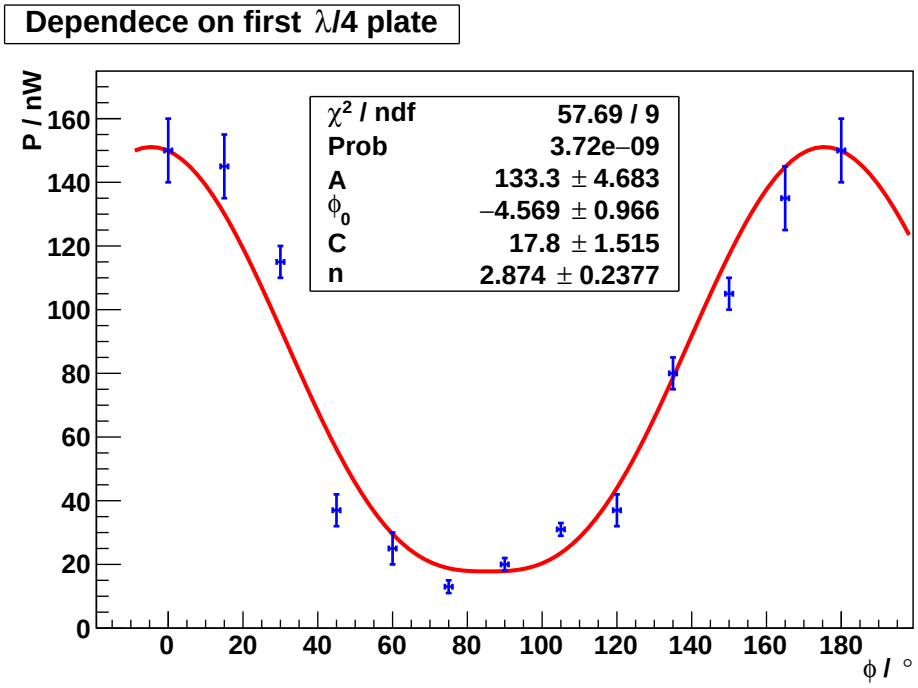

Figure 2.12.: The data obtained for the power in dependence of the angle of the first quarter waveplate and a fitted function to these values with a $\cos^n$-behavior.

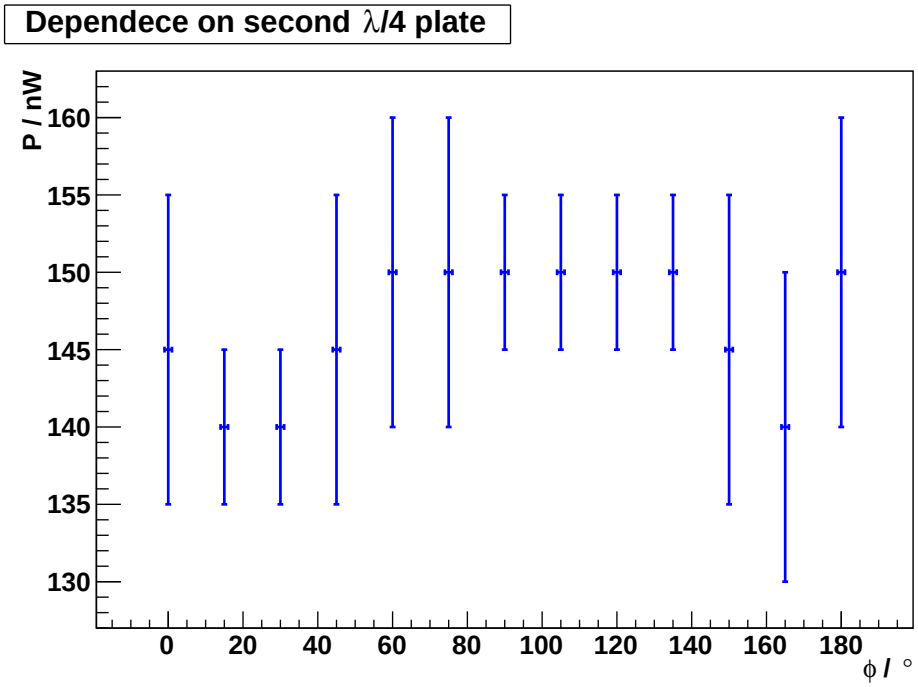

Figure 2.13.: The data obtained for the power in dependence of the angle of the second quarter waveplate. This results in an approximately constant behavior.

2.5 Changing the Magnetic Field

Besides the influence of the quarter waveplates on the fluorescence power of the MOT, we also want to inspect the influence of the current in the coils generating the magnetic field on the fluorescence power. We start at the maximum value of $I_{\text{coils}} = 5.2\,\text{A}$ and decrease this value until the power meter does not measure fluorescence anymore and thus the MOT disappears. The raw data we obtain is given in table B.4 in the appendix B. Plotting these values, we obtain figure 2.14, where we fitted a linear equation of the form

$$P(I) = m \cdot I + b$$

to these values, leaving out the first measured outliers. The linear behavior can be justified by considering the magnetic field B generated by the coils in anti-Helmholtz configuration, being proportional to the current I. Therefore, the restoring force is linear in the current I (see [5, p. 193]).

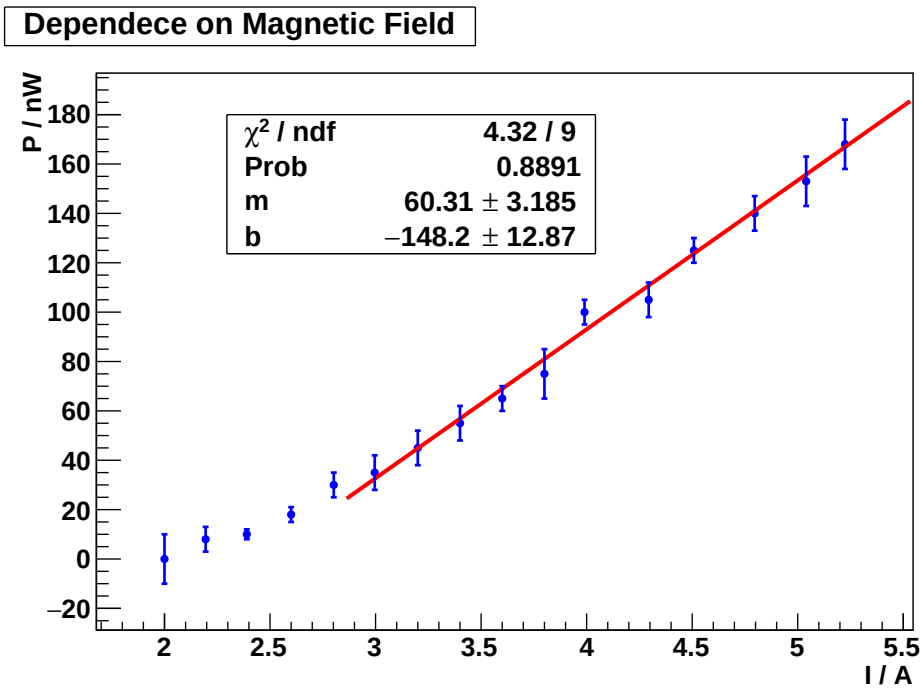

Figure 2.14.: The data obtained for the power in dependence of the current in the coils and a fitted linear equation to these values, where we left out some outliers.

2.6 Loading Behavior

To measure the loading behavior of the MOT, a photodiode is installed at the end of the tube instead of the power meter. The photodiode's output is displayed on a digital oscilloscope. When the magnetic field is turned on, a loading curve as depicted in figure 2.15 can be observed. This behavior can be quantified by

$$N(t) = N_0 \left(1 - \exp\left(-\frac{t}{\tau}\right)\right), \tag{2.14}$$

as given in [2]. A function of the form eq. (2.14) is fitted to the measured data and the loading time constant τ is extracted.

To improve the result, the procedure is repeated and the weighted mean value of these measurements is calculated. The corresponding plots and fits are given in figures C.1 and C.2 in appendix C and the resulting weighted mean value is

$$\tau = (0.02634 \pm 0.00064)\,\mathrm{s}.$$

At low pressure, the time constant can be a small fraction of 1 s, as mentioned in [2].

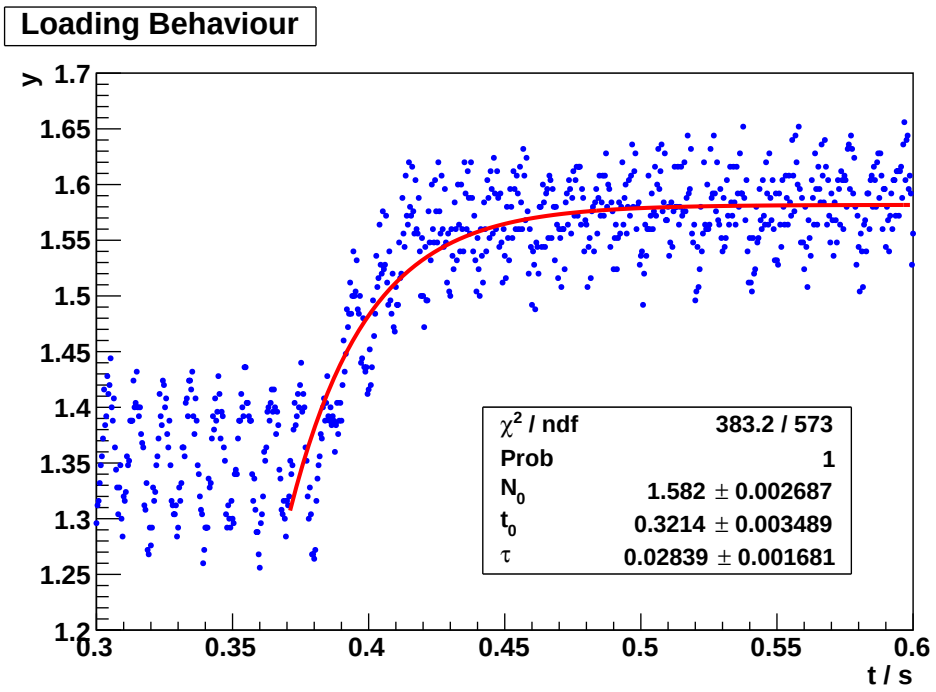

Figure 2.15.: The loading behavior of the MOT, generically shown for one of the several measurements.

Since the loading behavior is mainly determined by collisions of Rubidium atoms in the cavity, the atomic collision cross section σ_{Rb} of Rubidium can be calculated from the loading time τ. From [2], the relation between these value is given by

$$\frac{1}{\tau} = n_{\mathrm{Rb}} \sigma_{\mathrm{Rb}} v_{\mathrm{Rb}} \tag{2.15}$$

with the density n_{Rb} and mean velocity v_{Rb}. Using the equations for density and velocity of an ideal gas – which should be a good approximation – given by

$$v_{\mathrm{Rb}} = \sqrt{\frac{2k_B T}{m_{\mathrm{Rb}}}}, \qquad n_{\mathrm{Rb}} = \frac{p}{k_B T},$$

the collision cross section is given by

$$\sigma_{\mathrm{Rb}} = \sqrt{\frac{k_B T m_{\mathrm{Rb}}}{2p^2 \tau^2}}. \tag{2.16}$$

Here, k_B is the Boltzmann constant, $T = (297.05 \pm 1.00)\,\mathrm{K}$ the measured room temperature, $p = (4.5 \pm 0.5)\,\mu\mathrm{Pa}$ the pressure determined from the current of the

pump $I_{\text{pump}} = 0.01\text{mA}$ and $m_{\text{Rb}} = 1.41 \times 10^{-25}\,\text{kg}$ the mass[1] of ^{85}Rb. The cross section is then determined to be

$$\sigma_{\text{Rb}} = (1.43 \pm 0.16) \times 10^{-16}\,\text{m}^2,$$

which is of the same order as the value in [8], $\sigma_{\text{Rb}}^{\text{lit}} = 3 \times 10^{-13}\,\text{cm}^2$. This is also close to the theoretical value from dipole-dipole scattering given in [8], $\sigma_{\text{Rb}}^{\text{theo}} = 3.2 \times 10^{-13}\,\text{cm}^2$.

2.7 Detuning of the Laser Frequencies

By scanning through the cooling laser's frequency range and measuring the fluorescence of the MOT, the detuning can be determined. Here, a low frequency triangular signal is controlling the cooling laser to ensure that the MOT has enough time to load, while the repumping laser is locked. The MOT's response is observed with a photodiode. The signal of the photodiode and the cooling laser's spectrum are then compared with an oscilloscope. The frequency and amplitude of the triangular signal are adjusted in order to optimize the fluorescence, but a flickering of the MOT could not be observed with the camera.

The measured laser's spectrum signal can be seen in figure 2.16. It is blurred and consists of different overlaid lines. Therefore, only every fifth point is plotted, starting from the first, second, etc., leading to five graphs as also depicted in 2.16. These signals are much cleaner, showing a similar but shifted curve, and allow to identify the peaks. The fluorescence signals also improve in this way, such that this method will be used in the following.

To determine the detuning, a frequency calibration is needed, as the x-axis of the oscilloscope corresponds to a time. Since this is not of interest, no unit will be given. A superposition of three Gaussian curves with a quadratic background is fitted to the spectra, as can be seen in figure 2.17. In fact, a Lorentzian curve should be used but since only the peak position is of interest, a Gaussian curve is sufficient. For a better accuracy, one also should have fitted curves to all five spectra of one measurement (note that we only took every fifth point), but for simplicity, we decided for the conducted procedure.

With [1], the double peak can be identified as the $F \to F' = 3 \to 2$ and $F = 3 \to F' = 3$ transitions with a frequency difference of $\Delta f = 31.7\text{MHz}$. The calibration

[1] see https://en.wikipedia.org/wiki/Isotopes_of_rubidium

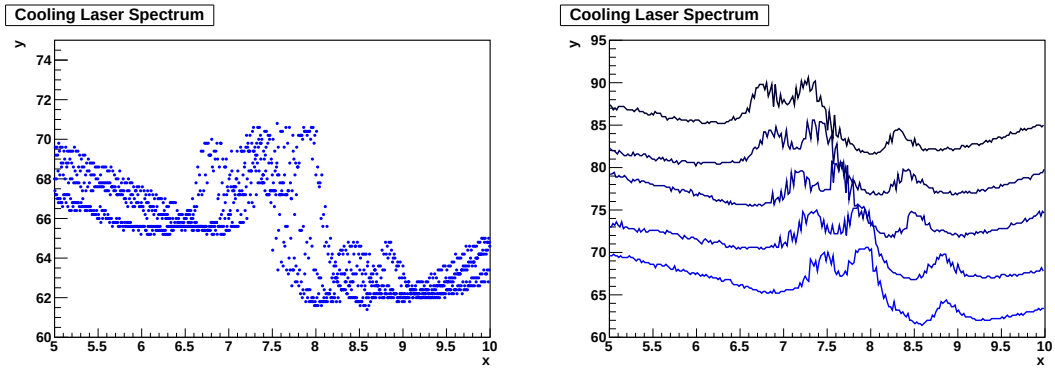

Figure 2.16.: The cooling laser's spectrum signal. The left graph shows the whole measured spectrum, while in the right graph only every fifth point is plotted, starting from the first, second etc., leading to five graphs. An offset in y-direction is used for distinction.

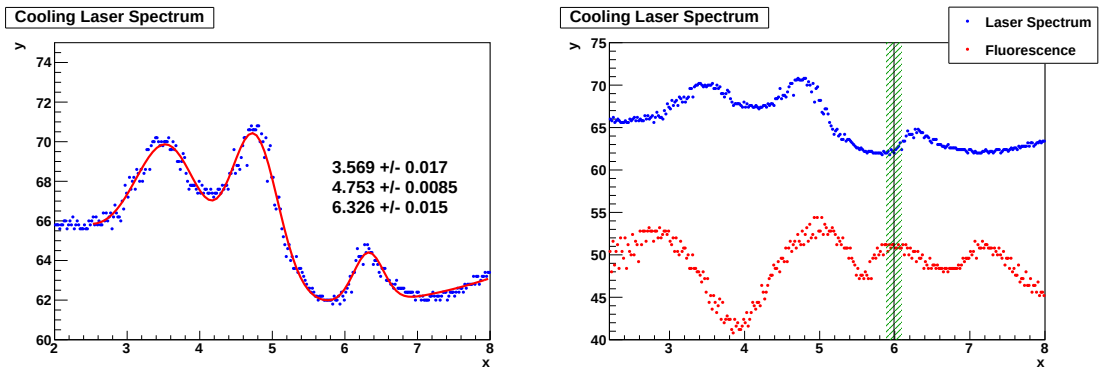

Figure 2.17.: Graphs used for the determination of the detuning. The left graph shows the fitted spectrum and the right graph shows the fluorescence peak of the MOT in comparison to the cooling laser's spectrum. Here, a rescaling and shift of the fluorescence signal is used.

factor from time to frequency differences can then be calculated as

$$C = \left| \frac{\Delta f}{x_1 - x_2} \right| \tag{2.17}$$

Now, the detuned fluorescence peak of the $F \to F' = 3 \to 4$ transition is identified as can be seen in figure 2.17, where the fluorescence signal is rescaled and shifted for a better comparison with the laser spectrum. The peak position is identified by eye, since it is difficult to fit a Gaussian curve to these values. The results are listed in table 2.1. The detuning can then be calculated from the difference of the $F = 3 \to F' = 4$ transition peaks in laser- and fluorescence spectrum

$$\Delta = C|x_{\text{laser}} - x_{\text{detune}}|. \tag{2.18}$$

To improve the result, this procedure is repeated for four more spectra from different measurements, as seen in figures C.3-C.6 in appendix C. The determined detuning Δ can also be found in table 2.1. Taking the weighted mean results in

$$\Delta = (13.1 \pm 2.1)\text{MHz}.$$

No.	Peak position [s]	Detuning [MHz]
1	5.99 ± 0.10	9.0 ± 2.7
2	6.57 ± 0.15	27.4 ± 9.2
3	8.13 ± 0.10	18.7 ± 6.1
4	6.68 ± 0.10	16.2 ± 6.9
5	4.62 ± 0.10	18.5 ± 5.6

Table 2.1.: The identified peak position and the corresponding detuning for the different measurements.

A redshift of 13 MHz is also used in [9, p. 27]. The big error is dominated by the error of the peak position in the fluoresence spectrum and could have been optimized by using more spectra.

The same experimental setup can be used to determine the influence of the repumping laser's frequency, with the cooling laser locked. Here, a flickering can be observed on the camera with the signal on the oscilloscope being cleaner than for the cooling laser. Figure 2.18 shows the recorded repumping laser's and the fluorescence spectrum which is shifted and rescaled again.

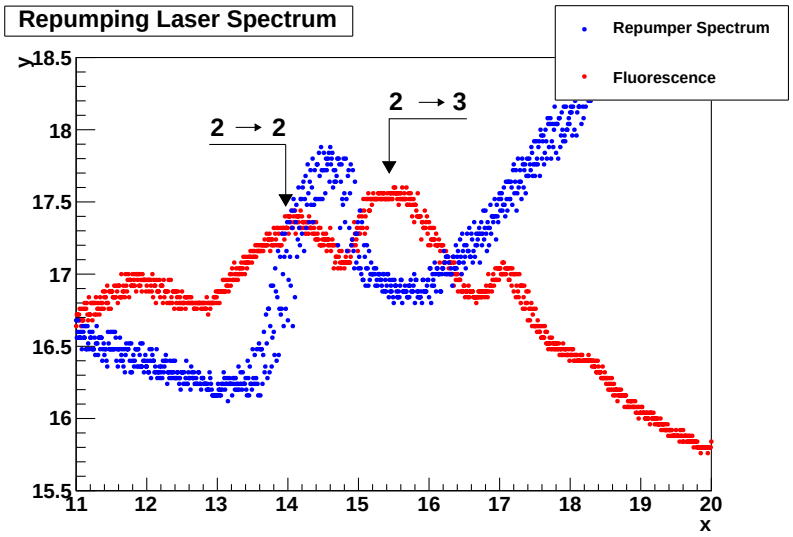

Figure 2.18.: Graphs used for the determination of the detuning. The left graph shows the fitted spectrum and the right graph shows the fluorescence peak of the MOT in comparison to the repumping laser's spectrum. Here, a rescaling and shift of the fluorescence signal is used.

While the laser spectrum only shows one peak, more peaks can be observed n the fluorescence spectrum, among which two are significantly higher. The peak in the laser spectrum is a superposition of the transitions $F = 2 \rightarrow F' = 1; 1, 2; 2; 1, 3; 2, 3$, as well as $F' = 3$, which has greater distance to the other peaks but also a small intensity and is thus hard to distinguish. The two bigger peaks in the fluorescence spectrum are therefore identified as the transitions $F = 2 \rightarrow F' = 2$ and $F = 2 \rightarrow F' = 3$ respectively, which are needed to make the MOT work, while the other peaks may be crossover peaks. Thus for the repumping laser, only a small detuning can be observed.

3 Conclusion

In this experiment, we used a laser system and a magneto-optical trap setup in order to catch atoms in said magneto-optical trap. After tuning and locking the cooling and repumping laser to the correct frequency, as well as having adjusted the incoming and back-reflected beams such that they exactly overlay in the middle of the vacuum chamber, we were able to inspect a magneto-optical trap (cloud of atoms) upon turning on the current $I = 5.2\,\mathrm{A}$ in the coils and detuning the cooling laser slightly to the red. Our cooling beam in the magneto-optical trap setup with $P_{\mathrm{beam}} = (6.7 \pm 0.1)\,\mathrm{mW}$ was split into three beams with each having a power of $P_{i=1,2,3} = 2.2\,\mathrm{mW}$. This is in accordance with the value of $P = 10\,\mathrm{mW}$ generically given in [1]. An improvement could have been made by readjusting the laser system.

When characterizing the magneto-optical trap, we found a mean value of $P_{\mathrm{tot}} = (30.4 \pm 3.4)\,\mu\mathrm{W}$ for the fluorescence power, a detuning of $\Delta = (13.1 \pm 2.1)\,\mathrm{MHz}$ and a beam diameter of $w = (0.247 \pm 0.061)\,\mathrm{cm}$. While the detuning is in accordance with the value given in [9], the fluorescence power is only half as large as the recommended value in [1]. An improvement could have been made by readjusting the mirrors and waveplates or improving the laser's red-shift with the offset knob. With these values, we were able to determine the population of the magneto-optical trap to be $N = (1.01 \pm 0.11) \times 10^7$ particles, which is in the same order of magnitude as the value $N_{\mathrm{lit}} = 4\ \times 10^7$ particles given in [2]. We determined the size of the magneto-optical trap twice – at different times – to be $\mathrm{MOT}_1 : (1.17 \pm 0.03)\,\mathrm{mm} \times (0.67 \pm 0.03)\,\mathrm{mm}$ and $\mathrm{MOT}_2 : (1.20 \pm 0.03)\,\mathrm{mm} \times (0.93 \pm 0.03)\,\mathrm{mm}$, where the second one had a rather round shape and was hypothesized as a sphere with diameter $d = (1.07 \pm 0.03)\,\mathrm{mm}$. When inspecting the dependence of the magneto-optical trap's fluorescence power on the angle of the quarter waveplates, we found the expected $\cos^2$-like behavior for one of the anterior waveplates and the expected constant behavior for one of the posterior waveplates. For the dependence on the current in the coils generating the magnetic field, we found a linear relationship. For the loading behavior, we determined a loading time of $\tau = (0.02634 \pm 0.00064)\,\mathrm{s}$ and finally an Rb-Rb cross section of $\sigma_{\mathrm{Rb}} = (1.43 \pm 0.16) \times 10^{-16}\,\mathrm{m}^2$, in accordance with the value in [8].

A Statistical Methods

Following [11], we want to summarize how to calculate a weighted mean for physical measurements. Taking N measurements $x_1, \ldots, x_N$ with errors $\epsilon_1, \ldots, \epsilon_N$, the weighted mean is defined as

$$x_{\mathrm{m}} = \frac{\sum_{i=1}^{N} w_i x_i}{\sum_{i=1}^{N} w_i} \quad \text{where} \quad w_i = \frac{1}{\sigma_i^2}. \tag{A.1}$$

The error on this mean is given by

$$\epsilon_m = \frac{1}{\sqrt{\sum_{i=1}^{N} w_i}}. \tag{A.2}$$

Peculiarly is here, that with the weights defined like this, more precise measurements count more than less precise measurements.

B Tables

Position on Rail [cm]	Power [mW]
39.0 ± 0.025	2.08 ± 0.00
39.1 ± 0.025	2.08 ± 0.00
39.2 ± 0.025	2.08 ± 0.00
39.3 ± 0.025	2.08 ± 0.00
39.4 ± 0.025	2.07 ± 0.00
39.5 ± 0.025	1.96 ± 0.00
39.6 ± 0.025	1.43 ± 0.00
39.7 ± 0.025	0.81 ± 0.00
39.8 ± 0.025	0.33 ± 0.00
39.9 ± 0.025	0.10 ± 0.00
40.0 ± 0.025	0.02 ± 0.00
40.1 ± 0.025	0.00 ± 0.00
40.2 ± 0.025	0.00 ± 0.00

Table B.1.: The measured power of 'the' laser beam (blue beam in figure 2.2) in dependence of the razor blade's position on the optical rail. With this measurement, we determine the diameter of the laser beam. The error on the fluorescence power is neglectable, due to no fluctuations.

Angle of anterior Quarter Waveplate [°]	Power [nW]
180 ± 1	150 ± 10
165 ± 1	135 ± 10
150 ± 1	105 ± 5
135 ± 1	80 ± 5
120 ± 1	37 ± 5
105 ± 1	31 ± 2
90 ± 1	20 ± 2
75 ± 1	13 ± 2
60 ± 1	25 ± 5
45 ± 1	37 ± 5
30 ± 1	115 ± 5
15 ± 1	145 ± 10
0 ± 1	150 ± 10

Table B.2.: The measured power of the MOT's fluorescence in dependence of the angle of the quarter waveplate passed by one of the incoming and the respective back-reflected beam. With this measurement, we confirm a Malus's law like behavior.

Angle of posterior Quarter Waveplate [°]	Power [nW]
180 ± 1	150 ± 10
165 ± 1	140 ± 10
150 ± 1	145 ± 10
135 ± 1	150 ± 5
120 ± 1	150 ± 5
105 ± 1	150 ± 5
90 ± 1	150 ± 5
75 ± 1	150 ± 10
60 ± 1	150 ± 10
45 ± 1	145 ± 10
30 ± 1	140 ± 5
15 ± 1	140 ± 5
0 ± 1	145 ± 5

Table B.3.: The measured power of the MOT's fluorescence in dependence of the angle of the quarter waveplate passed by one of the back-reflected beams. With this measurement, we confirm a constant relation between the angle and the power.

Current I of the Coils [A]	Voltage U [V]	Power [nW]
5.224 ± 0.001	8.13 ± 0.02	168 ± 10
5.040 ± 0.001	7.67 ± 0.00	153 ± 10
4.796 ± 0.001	7.33 ± 0.01	140 ± 7
4.508 ± 0.001	6.93 ± 0.01	125 ± 5
4.294 ± 0.001	6.66 ± 0.01	105 ± 7
3.990 ± 0.001	6.18 ± 0.01	100 ± 5
3.800 ± 0.001	5.85 ± 0.01	75 ± 10
3.600 ± 0.001	5.53 ± 0.01	65 ± 5
3.400 ± 0.001	5.14 ± 0.00	55 ± 7
3.200 ± 0.001	4.81 ± 0.01	45 ± 7
2.996 ± 0.001	4.47 ± 0.01	35 ± 7
2.802 ± 0.001	4.20 ± 0.01	30 ± 5
2.600 ± 0.001	3.86 ± 0.01	18 ± 3
2.394 ± 0.001	3.58 ± 0.01	10 ± 2
2.195 ± 0.001	3.27 ± 0.01	8 ± 5
2.000 ± 0.001	2.96 ± 0.01	0 ± 10

Table B.4.: The measured power of the MOT's fluorescence in dependence of the current in the coils generating the magnetic field.

C Figures

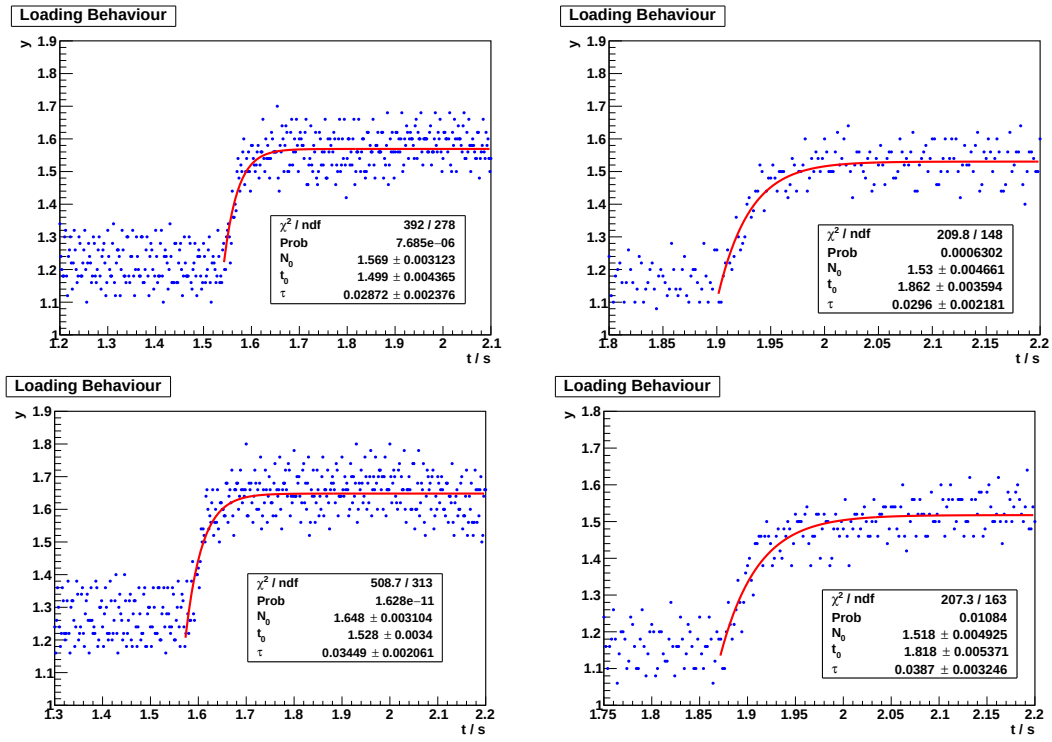

Figure C.1.: The loading behavior of the MOT, here shown for four additional measurements.

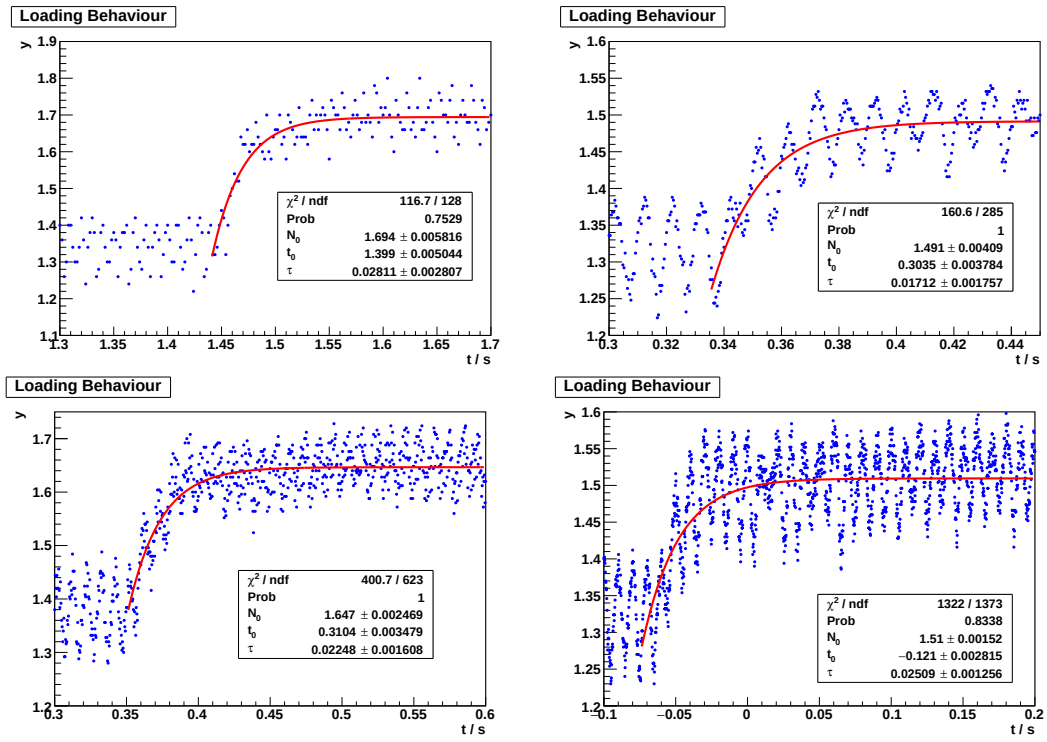

Figure C.2.: The loading behavior of the MOT, here shown for four additional measurements.

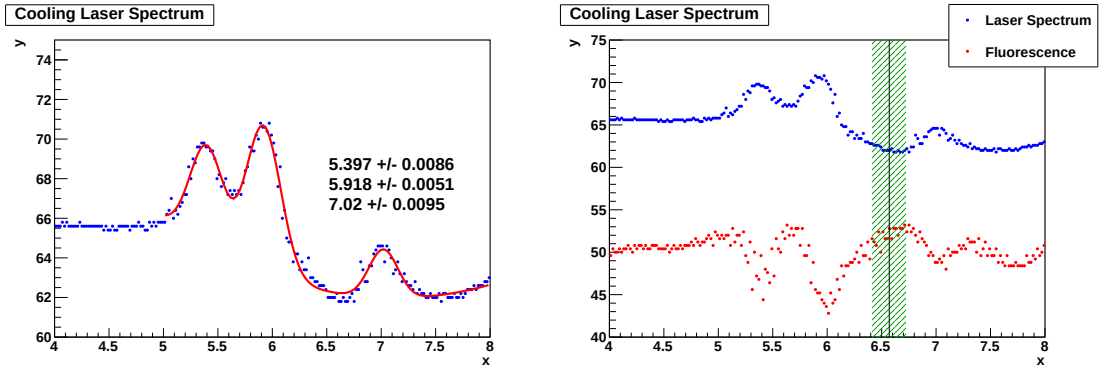

Figure C.3.: Graphs used for the determination of the detuning. The left graph shows the fitted spectrum and the right graph shows the fluorescence peak of the MOT in comparison to the cooling laser's spectrum. Here, a rescaling and shift of the fluorescence signal is used.

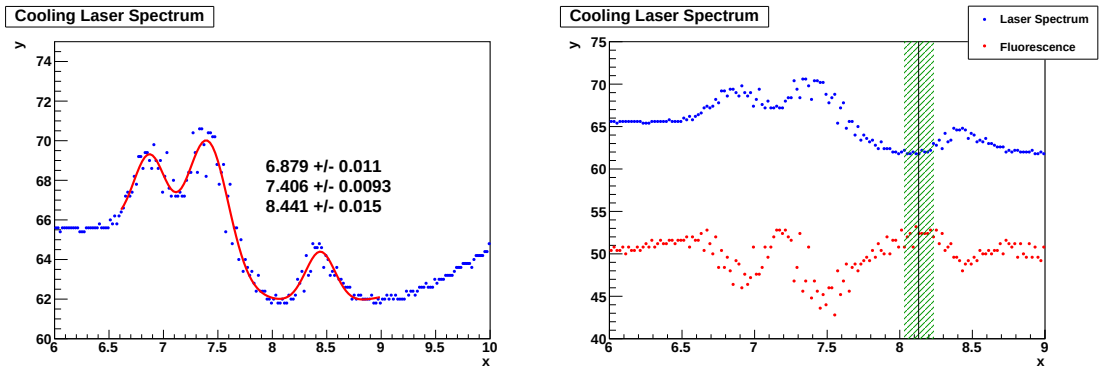

Figure C.4.: Graphs used for the determination of the detuning. The left graph shows the fitted spectrum and the right graph shows the fluorescence peak of the MOT in comparison to the cooling laser's spectrum. Here, a rescaling and shift of the fluorescence signal is used.

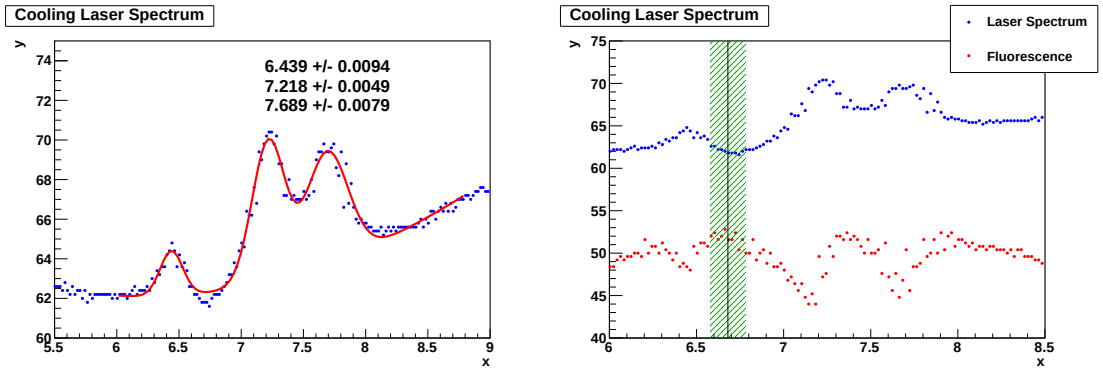

Figure C.5.: Graphs used for the determination of the detuning. The left graph shows the fitted spectrum and the right graph shows the fluorescence peak of the MOT in comparison to the cooling laser's spectrum. Here, a rescaling and shift of the fluorescence signal is used.

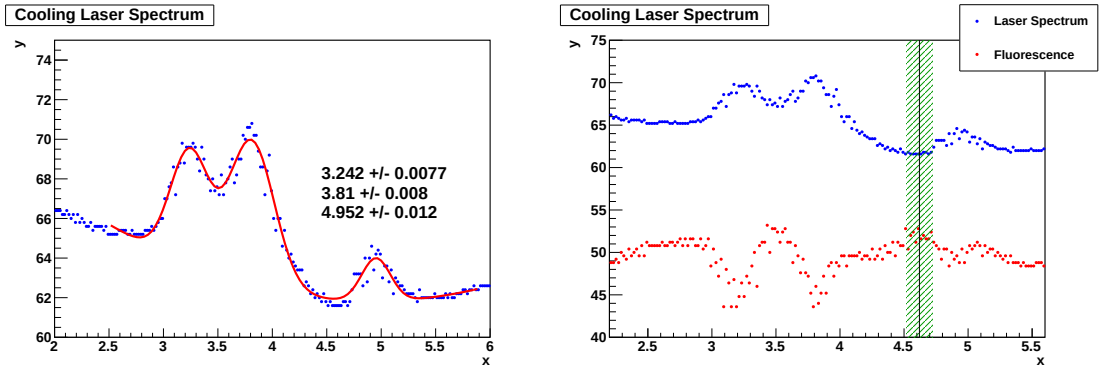

Figure C.6.: Graphs used for the determination of the detuning. The left graph shows the fitted spectrum and the right graph shows the fluorescence peak of the MOT in comparison to the cooling laser's spectrum. Here, a rescaling and shift of the fluorescence signal is used.

Bibliography

[1] University of Bonn. *Advanced Laboratory Course physics601, E214: The ATLAS Experiment (Properties of W Bosons and the Search for New Physics) – Additional Information handed out.* And references in this booklet.

[2] C. Wieman, G.Flowers and S.Gilbert. *Inexpensive Laser Cooling and Trapping Experiment for undergraduate Laboratories.* American Journal of Physics 63, 317 (1995). https://doi.org/10.1119/1.18072 (not the original link, as it is offline).

[3] Thomas Rieger and Thomas Volz. *Doppler-Free Saturation Spectroscopy.* Max-Planck-Institut für Quantenoptik, Garching. https://www.mpq.mpg.de/4992695/saturation_spectroscopy.pdf.

[4] Dieter Meschede. *Optics, Light and Lasers. The Practical Approach to Modern Aspects of Photonics and Laser Physics.* WILEY-VCH Verlag GmbH & Co. KGaA, 2004.

[5] C. J. Foot *Atomic Physics.* OXFORD University Press, 2005.

[6] Bartman. Example: Steradian cone in sphere, 2016. http://www.texample.net/tikz/examples/steradian-cone-sphere/.

[7] *Gaussian Beam Optics.* CVI Melles Griot. http://experimentationlab.berkeley.edu/sites/default/files/MOT/Gaussian-Beam-Optics.pdf.

[8] U. D. Rapol, A. Wasan and V. Natarajan. *Loading of a Rb magneto-optic trap from a getter source.*. Physical Review A, Volume 64. https://journals.aps.org/pra/pdf/10.1103/PhysRevA.64.023402.

[9] Tauschinsky, F.A. *Rydberg atoms on a chip and in a cell.* University of Amsterdam. https://pure.uva.nl/ws/files/2305591/126961_thesis.pdf.

[10] University of Bonn. *Advanced Laboratory Course (physics601), Description of Experiments: E214 ATLAS*. (Blue booklet). May 2012.

[11] University of Colorado, Minhyea Lee. PHYS2150 Experimental Physics, Spring 2018
`https://www.colorado.edu/physics/phys2150/phys2150_sp14/phys2150_lec4.pdf`.